Thin Solid Films 519 (2011) 5962–5965

Contents lists available at ScienceDirect

Thin Solid Films

journal homepage: www.elsevier.com/locate/tsf

Insights for void formation in ion-implanted Ge

B.L. Darby [a,*], B.R. Yates [a], N.G. Rudawski [a], K.S. Jones [a], A. Kontos [b], R.G. Elliman [c]

[a] Department of Materials Science and Engineering, University of Florida, Gainesville, FL 32611–6400, USA
[b] Varian Semiconductor Equipment Associates, Gloucester, MA 01930, USA
[c] Department of Electronic Materials Engineering, Research School of Physical Sciences and Engineering, Australian National University, Canberra, Australian Capital Territory 0200, Australia

ARTICLE INFO

Article history:
Received 4 October 2010
Received in revised form 10 March 2011
Accepted 15 March 2011
Available online 31 March 2011

Keywords:
Germanium
Annealing
Voids
Ion implantation
Transmission electron microscopy

ABSTRACT

The formation of voids in ion-implanted Ge was studied as a function of ion implantation energy and dose. (001) Ge substrates were self-implanted at energies of 20–300 keV to doses of 1.0×10^{13}–1.0×10^{17} cm^{-2}. Transmission electron microscopy revealed clusters of voids just below the surface for implant energies ≤120 keV at a dose of 2.0×10^{15} cm^{-2} and complete surface coverage for an implant energy of 130 keV and doses $\geq 1.0\times10^{16}$ cm^{-2}. Void clusters did not change in size or density after isothermal annealing at 330 °C for 176 min. The initial void formation is discussed in terms of the vacancy clustering and "microexplosion" theories with a damage map detailing the implant conditions necessary to produce voids.

© 2011 Elsevier B.V. All rights reserved.

1. Introduction

There is renewed interest in Ge as an alternative channel material in complementary metal-oxide-semiconductor devices due to its higher free carrier mobility and dopant activation compared to Si. However, the evolution of damage in ion-implanted Ge as a function of implantation conditions remains poorly understood. It is known that for a critical dose, Ge undergoes a crystalline (c-Ge) to amorphous (α-Ge) phase transition [1], and at significantly higher doses exhibits voiding within the α-Ge layer forming a porous structure with surface cavitation [2–6]. However, the threshold ion implantation conditions for void formation remain basically unknown.

Over the past 30 years, there has been much debate as to what mechanism governs the formation of the porous structure in ion-implanted Ge. Currently, there are two main theories of void formation for Ge: vacancy clustering and so-called "microexplosions". The vacancy clustering theory invokes the inefficient recombination of Ge point defects during ion-implantation [7], where once a critical point defect population is created by ion-implantation, excess vacancies cluster into pores [3,8–13] in order to minimize the dangling bond density. In contrast, the microexplosion theory is based on the creation of voids through pressure waves and thermal spikes caused by the overlap of ion cascades [6,14–16]. In principle, it is possible to determine which theory better models void formation by selecting appropriate implant conditions and observing the resulting microstructure after implantation. If vacancy clustering is the governing mechanism, then varying depth and concentration of the vacancy profile should have an effect on the size and depth of the voids. If the microexplosion theory governs the formation process, then a small fraction of implanted ions (<0.1%) would produce microexplosions that result in voids. This implies that dose is the critical parameter that controls the void formation process, which should occur at the surface regardless of the implant energy [14–16]. In this work, the influence of ion dose and implant energy on void formation in ion-implanted Ge is investigated in an attempt to better understand the threshold conditions for the formation of a porous microstructure as well as which theory best explains void formation in Ge.

2. Experimental details

Two sets of (001) Ge samples with background B concentrations of 5.0×10^{17} cm^{-3} were self-implanted at room temperature using a VIISta 900XP ion-implanter with beam current density of 0.38 μA/cm^2. The first set of samples was implanted at implant energies ranging from 20 to 300 keV with doses ranging from 1.0×10^{13}–1.0×10^{15} cm^{-2} while the second set was implanted with ion energies of 30–150 keV at a fixed dose of 2.0×10^{15} cm^{-2}. The samples were then annealed at 330 °C in a tube furnace in N_2 ambient for 22–176 min. A third set of samples was self-implanted at 130 keV with doses between 1.0×10^{16} and 1.0×10^{17} cm^{-2} using a 5SDH-4 tandem accelerator at Australian National University. Implantation for this set was performed at room temperature using a beam current density of 0.14 μA/cm^2. The α-Ge layers and voids were characterized using a JEOL 2010F transmission electron microscope at 200 kV in cross-section (XTEM) and plan-view

* Corresponding author.
E-mail address: bdarby@ufl.edu (B.L. Darby).

0040-6090/$ – see front matter © 2011 Elsevier B.V. All rights reserved.
doi:10.1016/j.tsf.2011.03.040

(PTEM). An FEI DB235 focused ion beam (FIB) was used to prepare both XTEM and PTEM samples via a 30 keV Ga^+ beam. Scanning electron microscopy (SEM) was used to characterize the surface morphology of the samples at 5 kV.

3. Results

Fig. 1(a) shows an XTEM micrograph of a sample self-implanted at 90 keV to a dose of 2.0×10^{15} cm^{-2} exhibiting clusters of small voids 15 ± 6 nm in diameter just below the surface and an α-Ge layer 107 ± 3 nm thick (as measured in regions without voids). PTEM imaging of the same sample, shown in Fig. 1(b), indicates an average of 9 ± 4 voids per cluster. Approximately 0.07% of the surface of this sample was covered by voids. After annealing the sample in Fig. 1(b) at 330 °C for 176 min, the amorphous layer crystallized, but the void clusters remain with the same area distribution and size as shown in Fig. 1(c). This is consistent with prior reports indicating the stability of porous regions formed from high dose self-implantation upon annealing [2,4,17,18]. Behavior similar to that presented in Fig. 1 was also observed for other samples self-implanted at 30–120 keV to a dose of 2.0×10^{15} cm^{-2}. It is apparent from Fig. 1 that voids were not present uniformly across the entire sample, but were clustered randomly. This observation is surprising considering the dose uniformity is estimated at <1% across the sample [6]. Interestingly, the average depth of the voids (measured by XTEM) in samples self-implanted at energies of 30–120 keV to a dose of 2.0×10^{15} cm^{-2} appears to be independent of implant energy, as shown in Fig. 2. This is in contrast to the approximate linear dependence of the α-Ge layer thickness and depth of the vacancy concentration profile peak (R_d) with implant energy predicted with SRIM [19]. Furthermore, there is a complete lack of voids upon increasing the self-implantation energy to 150 keV.

Fig. 3 shows a damage map for self-implantation in Ge. The threshold dose for the formation of a continuous amorphous layer in Ge is 5.0×10^{13} cm^{-2} [1], while the threshold implant dose for void formation was determined to be 2.0×10^{15} cm^{-2} with an implant energy of 120 keV. No voids were observed in XTEM or PTEM above this implant energy or below this dose. This threshold dose compares well with the void threshold doses for ions of similar mass, such as As^+ and Ga^+ [20].

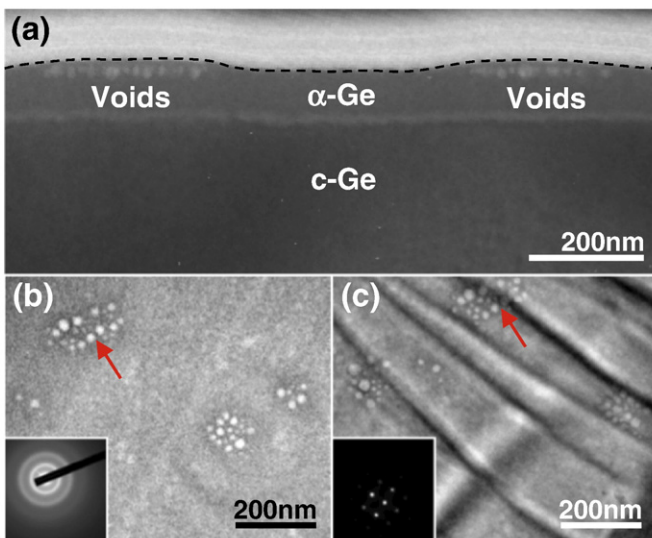

Fig. 1. (001) Ge self-implanted at 90 keV to a dose of 2.0×10^{15} cm^{-2}: a) XTEM micrograph of the as-implanted structure (surface indicated by the dotted line), b) PTEM micrograph of the as-implanted structure (inset diffraction pattern indicates sample is amorphous) and c) PTEM micrograph of the sample in b) following annealing at 330 °C for 176 min (inset diffraction pattern indicates sample is single crystal). Red arrows in parts b) and c) indicate the same void clusters in each sample.

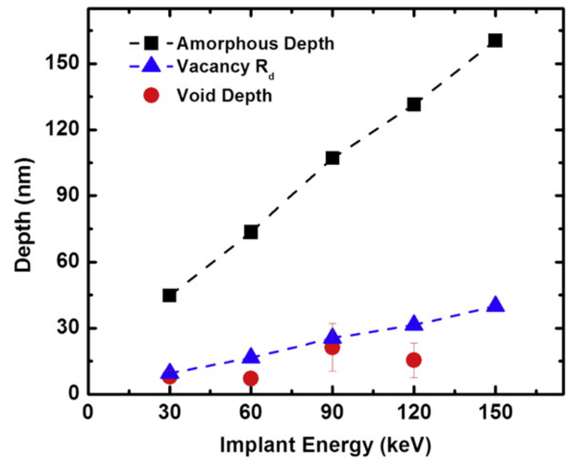

Fig. 2. Average void depth from the surface plotted against α-Ge thickness and depth of peak vacancy concentration (R_d) as determined by simulations [19]. Error bars indicate the average minimum and maximum depth of the voids versus implant energy for the samples self-implanted to a dose of 2.0×10^{15} cm^{-2}. No voids were observed at 150 keV with doses of 1.0×10^{14}–2.0×10^{15} cm^{-2}.

Fig. 4 presents the evolution of the porous microstructure with dose at implant energy of 130 keV. It is evident that the amorphous layer thickness remains relatively constant over the dose sequence, while the thickness of the porous region increases with dose, as shown in Figs. 4(a)–(c). The pore diameter also increases with dose as shown in the SEM micrographs presented in Fig. 4(d)–(f), which is consistent with literature reports [9]. Interestingly, the pores at the surface appear open at a dose of 1.0×10^{16} cm^{-2}, but an increasing portion of the pores get covered by a surface layer at 3.0×10^{16} and 1.0×10^{17} cm^{-2} as seen in Fig. 4(d)–(f). This leads to an undulating α/c interface since the ions travel through different thicknesses of material depending on whether a surface layer is present.

4. Discussion

If void formation is governed by a vacancy clustering mechanism alone one would expect a uniform void distribution due the high uniformity of the ion implantation process. This work has shown that

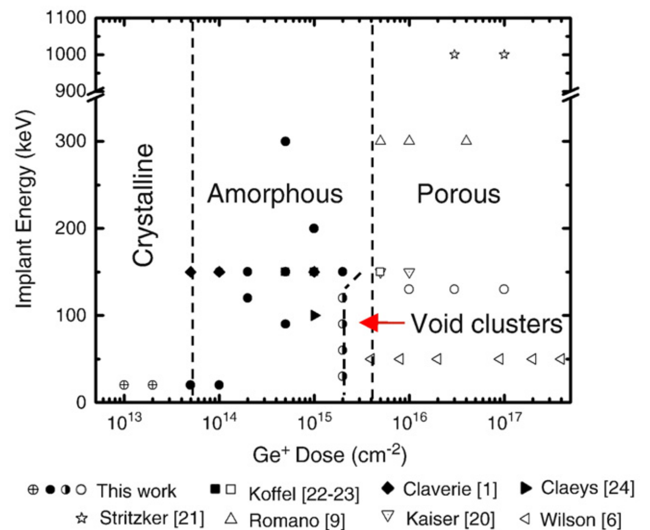

Fig. 3. Implant damage map for self implants into Ge: threshold dose values are 5.0×10^{13} cm^{-2} for amorphization, 2.0×10^{15} cm^{-2} for void formation, and 4.0×10^{15} cm^{-2} for porous structure formation. Boxed symbol represents crystallinity, filled symbols represent continuous amorphization, half-filled symbols represent void clustering, and open symbols represent porous formation. All implants were done at room temperature [1,6,9,20–24].

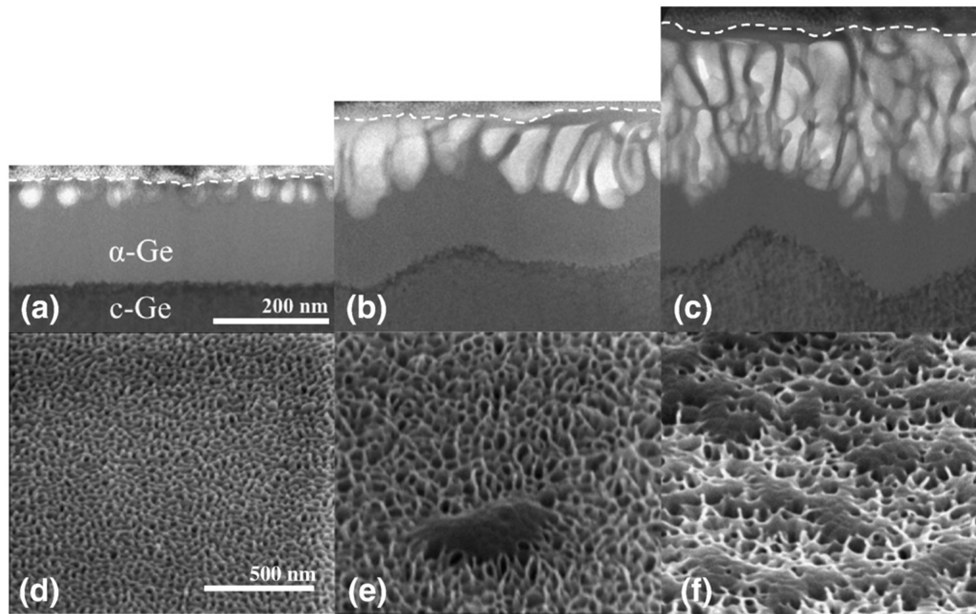

Fig. 4. XTEM micrographs illustrating the evolution of porous Ge with dose at 130 keV: a) 1.0×10^{16} cm^{-2}, b) 3.0×10^{16} cm^{-2}, c) 1.0×10^{17} cm^{-2} (surface indicated by dotted line) and corresponding plan view SEM micrographs taken at 52° d) 1.0×10^{16} cm^{-2}, e) 3.0×10^{16} cm^{-2}, f) 1.0×10^{17} cm^{-2}.

at a dose of 2.0×10^{15} cm^{-2}, approximately 0.07% of the surface is covered with clusters of voids. However, it is known that once the dose is increased to 4.0×10^{15} cm^{-2}, the entire surface is covered with voids [6]. By comparison, the microexplosion theory suggests ~0.1% of incoming ions overcome the critical energy to form a microexplosion. However, this cannot explain void formation alone since a two-fold increase in dose leads to an increase in surface coverage by roughly three orders of magnitude. The lateral range [19] (~15 nm) of a 90 keV Ge^+ ion into Ge is roughly equal to the average diameter of a single void (15 ± 6 nm), which means that the clusters of voids seen in Fig. 1 cannot be formed by a single ion. In addition, the voids observed in this work were several orders of magnitude larger than those predicted with single ion molecular dynamics simulations [14–16]. These results indicate that neither the vacancy clustering or microexplosion theory can solely explain void formation.

It is possible that the initial microexplosion serves as a nucleation point for vacancy clustering; once a single void is formed, the formation energy decreases for neighboring voids, resulting in a cluster. Therefore, the number of voids a cluster contains would increase with dose, resulting in even more nucleation points. In this manner, the percentage of the surface covered in voids would increase nonlinearly with dose after the initial void formation. Furthermore, it is known that the individual void size increases with dose [6,9], which strengthens the argument that voids nucleate through a microexplosion mechanism, and then a vacancy clustering mechanism could govern the growth process.

Additionally, the fact that voids were observed in the near surface region well above R_d indicates that vacancy clustering alone cannot explain void formation. If vacancy clustering solely governed void formation, then the void depth dependence on ion energy, shown in Fig. 2, should be centered on the vacancy R_d. Instead, the void depth is roughly the same value for all ion energies. In terms of the microexplosion explanation, there is a critical density of cascades required for a void to form. As the depth of the cascade increases, the cascade volume increases as well, and thus the critical energy to produce a microexplosion increases rapidly with the depth of the cascade below the surface [16]. This could possibly explain the observation of voids at the same distance from the surface, regardless of implant energy. It is possible that self-implantation at 150 keV to a dose of 2.0×10^{15} cm^{-2} produces a cascade density just below the critical value, thus resulting in no void formation at the surface.

Upon increasing the dose into the porous regime, several factors determine the surface morphology, including sputtering, redeposition, swelling, and ion beam annealing. It is likely that a combination of these factors contribute to the surface layer formation and surface roughness as shown in Fig. 4(d)–(f). Interestingly, the amorphous depth remains relatively constant, whereas the depth of the porous layer increases with dose. It is possible that vacancies continue to cluster with increasing dose, leaving the interstitials to migrate out from the surface, causing the surface to swell.

5. Conclusions

This work has shown that void formation in ion-implanted Ge does not occur uniformly across the surface of the samples. Rather, void formation at the threshold implant conditions exists in random clusters, which may be explainable via a combination of both the vacancy clustering and microexplosion theories of void formation. This work suggests that implant conditions must be chosen carefully in any type of Ge-based device processing; since common p- and n-type dopants (Ga^+ and As^+) have similar masses to Ge^+. Dopant doses that approach 2.0×10^{15} cm^{-2} could result in void formation at low implant energies which cannot be removed via annealing.

Acknowledgments

The authors acknowledge the Intel Corporation for funding this work and the Major Analytical Instrumentation Center at the University of Florida for use of the FIB, TEM, and SEM facilities.

References

[1] A. Claverie, S. Koffel, N. Cherkashin, G. Benassayag, P. Scheiblin, Thin Solid Films 518 (2010) 2307.
[2] E.M. Lawson, K.T. Short, J.S. Williams, B.R. Appleton, O.W. Holland, O.E. Schow, Nucl. Instrum. Methods Phys. Res. 209 (1983) 303.
[3] O.W. Holland, B.R. Appleton, J. Narayan, J. Appl. Phys. 54 (1983) 2295.
[4] B.R. Appleton, O.W. Holland, J. Narayan, O.E. Schow, J.S. Williams, K.T. Short, E. Lawson, Appl. Phys. Lett. 41 (1982) 711.
[5] B.R. Appleton, O.W. Holland, D.B. Poker, J. Narayan, D. Fathy, Nucl. Instrum. Methods Phys. Res. B 7–8 (1985) 639.

[6] I.H. Wilson, J. Appl. Phys. 53 (1982) 1698.
[7] R. Kogler, A. Mucklich, W. Skorupa, A. Peeva, A.Y. Kuznetsov, J.S. Christensen, B.G. Svensson, J. Appl. Phys. 101 (2007) 033508.
[8] H. Huber, W. Assmann, S.A. Karamian, A. Mucklich, W. Prusseit, E. Gazis, R. Grotzschel, M. Kokkoris, E. Kossionidis, H.D. Mieskes, R. Vlastou, Nucl. Instrum. Methods Phys. Res. B 122 (1997) 542.
[9] L. Romano, G. Impellizzeri, M.V. Tomasello, F. Giannazzo, C. Spinella, M.G. Grimaldi, J. Appl. Phys. 107 (2010) 084314.
[10] L. Ottaviano, A. Verna, V. Grossi, P. Parisse, S. Piperno, M. Passacantando, G. Impellizzeri, F. Priolo, Surf. Sci. 601 (2007) 2623.
[11] Y.J. Chen, I.H. Wilson, W.Y. Cheung, J.B. Xu, S.P. Wong, J. Vac. Sci. Technol., B 15 (1997) 809.
[12] S. Rubanov, P.R. Munroe, Micron 35 (2004) 549.
[13] M.C. Ridgway, C.J. Glover, K.M. Yu, G.J. Foran, C. Clerc, J.L. Hansen, A.N. Larsen, Phys. Rev. B 61 (2000) 12586.
[14] M. Ghaly, K. Nordlund, R.S. Averback, Philos. Mag. A 79 (1999) 795.
[15] J.C. Kim, D.G. Cahill, R.S. Averback, Surf. Sci. 574 (2005) 175.
[16] P. Bellon, S.J. Chey, J.E. Vannostrand, M. Ghaly, D.G. Cahill, R.S. Averback, Surf. Sci. 339 (1995) 135.
[17] L.M. Wang, R.C. Birtcher, Philos. Mag. A 234 Prop. 64 (1991) 1209.
[18] A. Satta, E. Simoen, T. Janssens, T. Clarysse, B. De Jaeger, A. Benedetti, I. Hoflijk, B. Brijs, M. Meuris, W. Vandervorst, J. Electrochem. Soc. 153 (2006) G229.
[19] J.F. Ziegler, Nucl. Instrum. Methods Phys. Res., Sect. B 219 (2004) 1027.
[20] R.J. Kaiser, S. Koffel, P. Pichler, A.J. Bauer, B. Amon, A. Claverie, G. Benassayag, P. Scheiblin, L. Frey, H. Ryssel, Thin Solid Films 518 (2010) 2323.
[21] B. Stritzker, R.G. Elliman, J. Zou, Nucl. Instrum. Methods Phys. Res., Sect. B 175 (2001) 193.
[22] S. Koffel, N. Cherkashin, F. Houdellier, M.J. Hytch, G. Benassayag, P. Scheiblin, A. Claverie, J. Appl. Phys. 105 (2009) 3.
[23] S. Koffel, P. Scheiblin, A. Claverie, G. Benassayag, J. Appl. Phys. 105 (2009) 013528.
[24] C. Claeys, E. Simoen, K. Opsomer, D.P. Brunco, M. Meuris, Mater. Sci. Eng. B 154 (2008) 49.